# Geostationary satellite observations of extreme methane emissions from a natural gas pipeline

Marc Watine-Guiu[1,2 ‖], Daniel J. Varon[1* ‖], Itziar Irakulis-Loitxate[3,4], Nicholas Balasus[1], Daniel J. Jacob[1]

[1] Harvard University, Cambridge, 02138, USA.
[2] ETH Zürich, 8092 Zürich, Switzerland.
[3] Universitat Politècnica de València, Valencia, Spain.
[4] International Methane Emissions Observatory, United Nations Environment Programme, Paris, France.

**Corresponding author:** *Daniel J. Varon

**Email:** danielvaron@g.harvard.edu

**Author Contributions:** ‖ M.W.G. and D.J.V. contributed equally to this work.

==========

**This is a non-peer reviewed preprint that is subject to change. Please feel free to contact the corresponding author; we welcome feedback.**

==========

**Abstract**

We demonstrate geostationary satellite monitoring of a large methane point source with the U.S. Geostationary Operational Environmental Satellite (GOES) constellation. GOES provides continuous 5–10-minute coverage of the Americas at 0.5–2 km nadir pixel resolution in 16 spectral bands. We use the shortwave infrared bands to track the full evolution of an extreme methane release from the El Encino – La Laguna natural gas pipeline in Durango, Mexico on 12 May 2019. The release lasted three hours at a variable rate of 260–550 metric tons of methane per hour and totaled 1130–1380 metric tons, enough to power 3600–4400 Mexican urban households for a year. We show how the time-dependent source rate can be estimated from a sequence of 5-minute GOES scans without the need for information on local wind speed. Our results demonstrate the unique value of geostationary satellite instruments for detecting extreme and brief methane emission events, quantifying emissions from variable point sources, and precisely determining source locations.

**Significance Statement**

Decreasing atmospheric methane emissions is an urgent priority to slow near-term climate change. Satellites have unique capabilities to pinpoint methane sources in support of climate action, but the current observing system is entirely in low-Earth orbit and thus incapable of monitoring diurnal variability and intermittency of emissions. Here we demonstrate continuous 5-minute monitoring of methane point emissions with the U.S. Geostationary Operational Environmental Satellite (GOES) constellation. We apply this to quantify an extreme methane release from a natural gas pipeline in Durango, Mexico, which lasted for three hours on 12 May 2019. Our techniques can be adapted to other geostationary satellite systems for Europe, Africa, and Asia to provide continuous monitoring of large and brief methane releases.

## Introduction

Methane is a short-lived greenhouse gas responsible for about one third of greenhouse radiative forcing since pre-industrial times (IPCC AR6, 2021). Anthropogenic methane emissions include major contributions from agriculture, oil and gas production, coal mining, and waste (Saunois et al., 2020). Mitigating methane emissions has become increasingly attractive as a strategy to slow near-term climate change (Ocko et al., 2021), with momentum building in recent years behind the 2021 *Global Methane Pledge* signed by more than 100 countries, the 2022 U.S. *Inflation Reduction Act* with measures to limit methane emissions from oil and gas production, and the 2023 *Fit for 55* plan to slash EU greenhouse gas emissions 55% from 1990 levels by 2030, among other efforts.

Satellite instruments sensitive to atmospheric methane have unique capabilities for monitoring emissions in support of climate action. They can quantify methane emissions from the global scale down to individual point sources by observing back-scattered sunlight in the shortwave infrared (SWIR; Jacob et al., 2016; 2022). However, the current fleet is entirely in low-Earth orbit, with revisit rates for areas of interest of one day at best. Nearly all of the instruments are sun-synchronous, with overpasses between 10:00 and 13:00 local solar time. This means that the current observing system is largely incapable of monitoring the diurnal variability and intermittency of methane emissions, which can lead to substantial bias in emission estimates (Vaughn et al., 2018; Cusworth et al., 2021; Lauvaux et al., 2022).

Here we show how the U.S. Geostationary Operational Environmental Satellites (GOES) with 0.5–2 km nadir pixel resolution can monitor very large methane point sources in the Americas with up to 5-minute continuous coverage. We apply this capability to track the full evolution of an extreme methane release from the El Encino – La Laguna natural gas pipeline in Durango, Mexico on 12 May 2019.

## Results

The release was first observed by the TROPOspheric Monitoring Instrument on 12 May 2019 (TROPOMI; Veefkind et al., 2012; Fig. S1) and reported at 372 t $h^{-1}$ by Lauvaux et al. (2022). This is comparable in instantaneous magnitude to historic methane releases such as the 2022 Nord Stream pipeline rupture (Jia et al., 2022). TROPOMI detected the plume near the El Encino – La Laguna (EELL) natural gas pipeline in Durango. The EELL pipeline is part of the Wahalajara pipeline system that supplies Mexico with natural gas from the U.S. Permian Basin (EIA, 2020). It transports 1.5 Bcf per day of natural gas from Chihuahua to Durango. On 11 May 2019, Sentinel-2 also detected large emissions near the pipeline and identified the source as a pipeline block valve station (26.08580N, 104.31682W; Fig. 1; Fig. S2). Block valve stations are used to isolate sections of natural gas pipelines during maintenance, emergency shutdowns, and release of excess pressure (Farzaneh-Gord et al., 2018). We focus our analysis here on GOES-West imagery of the EELL pipeline in Durango, with a viewing zenith angle of 23° and resulting pixel resolutions of 1.273 km and 2.547 km in the SWIR bands 5 and 6 from which we perform our GOES methane retrievals (Materials and methods).

Figure 1 shows the EELL pipeline source location along with a composite of GOES methane plume retrievals on 12 May 2019. Figures 1a–b show the location of the scene in northern Mexico and high-resolution surface imagery of the block valve station responsible for the observed methane release (26.08580°N, 104.31682°W), as determined by Sentinel-2 on 11 May 2019 (Fig. S2). Figure 1c illustrates the temporal evolution of the 12 May 2019 release with five hand-selected GOES snapshots of the resulting methane plume (also see Movies S1–2). We estimate the release lasted 3 hours, after which the plume extended more than 80 km from the source. The peak plume enhancement was 1325 ppb during this period, roughly 70% above atmospheric background levels. Figure S3 shows 48 GOES plume retrievals at 5-minute intervals over the full course of the event.

Figure 2 shows our quantification of the release volume and source rate. No plume was observed before 16:30 UTC. The release began at 16:30 UTC (11:30 local time) and ended at 19:30 UTC (14:30 local time). Clouds prevented viewing after 20:20 UTC. Sample MBMP methane retrieval fields are shown in Figures 2b–d along with the resulting plume masks (Materials and methods). The methane plume is clearly detectable above a noise floor of standard deviation 0.06 mol $m^{-2}$ (~9% precision), and the plume masks capture its spatiotemporal evolution. Figure 3a

shows the growth in integrated methane enhancement (IME [kg]; Materials and methods) over time. The IME increases rapidly in the first 2.5 hours of the release with an average source rate of 460 ± 90 t $h^{-1}$ (slope of regression line), comparable to the 372 t $h^{-1}$ reported by Lauvaux et al. (2022) from a single TROPOMI pass roughly one hour after the release ended. It stabilizes in the third hour around 19:00, as distant plume enhancements begin to diffuse below the mask detection limit. It then declines around 19:30 UTC following the end of the release, which we diagnose by visualization of the plume detaching from the source (Fig. 3d, S3). The blue line shows our estimate of the time-dependent source rate as the trend of a 5-point moving average of the IME. Emissions fluctuated between 260 and 550 t $h^{-1}$, with a gradual decline over the 2.5-hour fitting period. Extrapolating these source rate estimates over the full release yields similar estimates of total methane emissions, with 1380 t from the 460 t $h^{-1}$ source rate and 1130 t from the time-dependent source rate (area under curve). Assuming 80% methane content for Permian natural gas (Alvarez et al., 2018), this is enough to power 3600–4400 Mexican urban households (Molar-Cruz et al., 2022) for a year.

The 12 May 2019 release was not an isolated incident, as evidenced by the previous day's Sentinel-2 detection (Fig. S2). In fact, TROPOMI and Sentinel-2 detect large methane plumes from three different block valve stations along the EELL pipeline on 11 different days between 7 April 2019 and 24 May 2019 (Fig. S4–6), indicating extensive and prolonged operator activity. Five of the releases are from the block valve station shown in Figure 2, and the others occurred at stations within 65 km of that source on 6 other days (7 April 2019; 16 and 21–24 May 2019; Fig. S4–6). GOES detects emissions for all events, but cloud cover prevents quantification over the full durations of the releases except on 12 May 2019. We estimate source rates of ~140–340 t $h^{-1}$ from cloud-free GOES coverage on the other days (Fig. S6), demonstrating the unique capability of geostationary satellite instruments to observe during cloud-free periods of otherwise cloudy days.

**Discussion**

Our work illustrates the potential of geostationary satellites to provide continuous monitoring of large methane point sources. We showed how 5-minute GOES imagery enabled quantification of the duration, source variability, and total emission of a natural gas pipeline methane release previously detected by Lauvaux et al. (2022) as a single snapshot from TROPOMI observations. TROPOMI observed the plume roughly 50 minutes after the end of the release with an aliased origin more than 10 km downwind of the actual source location, and just before clouds set in. The continuous imaging from GOES illustrates the improved ability of geostationary observations to localize and quantify intermittent sources. Lacking better information, Lauvaux et al. assumed a default 24-hour duration for their instantaneous TROPOMI methane plumes observed on consecutive days to estimate total annual emissions. We show here that such events can occur over much shorter periods of time and with variable source rate, even when observed in the same location on consecutive days. This has major implications for previous estimates of total emissions from intermittent methane point sources: those estimates may be too high if typical releases are brief, or too low if low-Earth orbit satellites significantly underestimate the true number of releases. Geostationary satellite instruments have unique potential to help answer these questions.

The retrieval techniques we present here for GOES can be readily applied to other geostationary satellite systems with similar SWIR bands and revisit rates, including the Japanese Himawari constellation over Asia and Oceania (Bessho et al., 2016) and the European Meteosat Third Generation (MTG) constellation over Europe, Africa, and the Middle East (Holmlund et al., 2021). More work is needed to characterize the methane sensitivity of these instruments under different observing conditions, including variable surface types and sun-satellite geometries, and to what extent the methane retrievals can be improved to detect smaller sources.

Our results highlight the importance of developing dedicated geostationary satellite instruments to monitor greenhouse gasses. The GeoCarb instrument (Moore et al., 2018) planned for launch to geostationary orbit in 2025 was recently canceled. Until a successor mission is launched with better methane sensitivity, multispectral geostationary satellite systems like GOES will be of great value as early warning systems to identify extreme methane point sources and trigger further investigation with fine-scale methane imagers such as GHGSat, Sentinel-2, and EMIT.

## Materials and Methods

The top-of-atmosphere Level-1b (L1b) GOES radiance data are available at https://noaa-goes16.s3.amazonaws.com/index.html#ABI-L1b-RadC/.

### GOES satellite observations

GOES is a geostationary satellite constellation operated by the U.S. National Oceanic and Atmospheric Administration to monitor the land and atmosphere across the Americas. It comprises two satellites, GOES-East at 75.2°W and GOES-West at 137.2°W, which together provide full-disk (hemispheric) scans every 10 minutes and scans of the continental U.S. and parts of Canada and Mexico every 5 minutes. The GOES Advanced Baseline Imager (ABI) delivers multispectral imagery in 16 spectral bands from the visible to thermal infrared, with nadir pixel resolution of 0.5–2 km depending on the band (Schmit et al., 2017). Here we retrieve methane column enhancements (mol $m^{-2}$) from GOES ABI Level-1B (L1B) top-of-atmosphere reflectances in the SWIR bands 5 (~1590–1630 nm) and 6 (~2220–2270 nm), which have respective nadir pixel resolutions of 1 km and 2 km.

Figure 3 shows methane absorption cross-sections in the 1550–2450 nm SWIR spectral range, based on absorption line spectra from the HIgh-resolution TRANsmission (HITRAN2016; Kochanov et al., 2016; Gordon et al. 2017) molecular absorption database. Also shown are the GOES SWIR bands (bands 5 and 6), including position, width, and mean absorption cross-section. Band positions are comparable to those of the Sentinel-2 (20 m pixels) and Sentinel-3 (500 m pixels) multispectral satellite instruments with demonstrated methane sensitivity to large point sources (Varon et al., 2021; Irakulis-Loitxate et al., 2022; Pandey et al., 2023).

### GOES methane retrieval

We adapt the multi-band–multi-pass (MBMP) methane retrieval of Varon et al. (2021) to infer methane column enhancements (mol $m^{-2}$) from normalized reflectance differences between GOES bands 5 and 6 on different 5-minute scans of the EELL pipeline scene. GOES performed 84 scans of the study area between 14:00 and 21:00 UTC (9:00–16:00 local time) on 12 May 2019. For a scan of interest (target scan), the MBMP method requires identifying a plume-free reference scan under similar observing conditions with which to remove surface-related artifacts from the retrieval. For each scan starting at 14:00 UTC, we construct a reference scan from the average of the 7 scans that occurred within 15 minutes of the target-scan time on another day when no significant methane enhancement was observed.

The retrieval compares the target-scan reflectances $R_5$ and $R_6$ with the reference-scan reflectances $R_5'$ and $R_6'$. The first step is to compute the fractional difference in reflectance between bands for the target and reference scans:

$$\Delta R = \frac{cR_6 - R_5}{R_5}, \quad (1)$$

$$\Delta R' = \frac{c'R_6' - R_5'}{R_5'}, \quad (2)$$

where c and c' are scaling factors to remove scene-wide brightness differences between bands 5 and 6. To compute methane column enhancements $\Delta\Omega$ (mol $m^{-2}$), we compare $\Delta R$ and $\Delta R'$ to a fractional absorption model:

$$m(\Delta\Omega) \approx \frac{T_6(\Omega + \Delta\Omega)}{T_6(\Omega)} - \frac{T_5(\Omega + \Delta\Omega)}{T_5(\Omega)}, \quad (3)$$

where $T$ is the modeled top-of-atmosphere radiance. We use the 100-layer, clear-sky radiative transfer model of Varon et al. (2021) to simulate $T_5$ and $T_6$ in the GOES SWIR bands 5 (1590-1630) and 6 (2220-2300) at 0.02 nm resolution, accounting for variable viewing/solar zenith

angles and integrating over each band's spectral window. The model takes into account vertical profiles of methane, water vapor, and $CO_2$, from the U.S. Standard Atmosphere (Anderson et al., 1986). Absorption line spectra are from HITRAN2016. We use a Newton method to solve for $\Delta\Omega$ and for $\Delta\Omega'$ by minimizing $|\Delta R - m(\Delta\Omega)|$ and $|\Delta R' - m(\Delta\Omega')|$, and subtract the results to compute the MBMP methane enhancement:

$$\Delta\Omega_{MBMP} = \Delta\Omega - \Delta\Omega'. \quad (4)$$

This subtraction removes systematic surface-related errors in the retrieval by deleting artifacts present in both retrieval fields.

We used the GOES Clear Sky Mask (ACM) Level 2 product to mask out clouds when computing $\Delta R$ and $\Delta R'$. Small clouds sometimes go undetected and introduce error to the retrieval (e.g., bottom row of Figure S3). Ground shadows from the clouds are another source of retrieval artifacts. Future work could attempt to filter these out using metrics like the Structural SIMilarity Index (SSIMI; Wang et al., 2004) between retrieval and reference images, as proposed by Pandey et al. (2023) for Sentinel-3.

**Source rate retrieval**

Quantifying the source rate of a methane point source from satellite plume imagery first requires constructing a binary plume mask to separate methane enhancements from background noise. We mask our GOES methane plumes by hysteresis thresholding with low and high threshold (Groshenry et al., 2022). This incorporates pixels above the low threshold (50th percentile) when they are connected to pixels above the high threshold (95th percentile), including in the previous snapshot. We find that this dual-threshold approach smooths the evolution of the mask from scan to scan. We further apply a 3x3 median filter and manual post-processing as needed to smooth the mask edges.

After masking the plume across all satellite scans, we quantify the source rate by tracking the evolution of the integrated methane enhancement (IME) within the mask. The IME [kg] for a given scan is computed as (Frankenberg et al., 2016; Varon et al., 2018)

$$IME = m_{CH_4} \sum_{j=1}^{N} \Delta\Omega_j A_j, \quad (5)$$

where $m_{CH_4} = 0.01604$ [kg mol$^{-1}$] is the molar mass of methane, $\Delta\Omega_j$ [mol m$^{-2}$] is the methane column enhancement in the *j*th plume pixel, $A_j$ [m$^{-2}$] is the corresponding pixel area, and *N* is the total number of mask pixels. After computing the IME for all scans, we estimate source rate from the growth of IME over time, in two different ways: (1) as the slope of an ordinary least-squares regression line, which estimates the period-mean source rate, and (2) from the trend of the IME time series, which captures the time-dependent source rate. These approaches have the advantage of being independent of the local wind speed, which is typically the primary uncertainty in source rates retrieved from low-Earth orbit satellite observations (Varon et al., 2018; Gorroño et al., 2023). A disadvantage is that they do not account for turbulent diffusion at the mask edges, which would bias the source rate low if the plume is not well-contained within the mask. This bias, however, would be small for large sources during the plume's initial growth phase, when it is highly concentrated and easily distinguishable from the background (see Movies S1–2). To estimate uncertainty in the source rate, we perform the masking and quantification procedure using reference scans from 6 different dates when no significant methane enhancement was observed over the location (13, 17, 18, 19, 20, and 21 May 2019), and report the mean and standard deviation of results across the 6 estimates.

We estimate the beginning and end of the release directly from the satellite data by monitoring the near-field IME within the 3x3 pixel neighborhood of the source. We define the source as active when the near-field IME exceeds 10 t, until the plume detaches from the source. We compute the source rate regression line from the beginning of the event until the observed IME stabilizes when turbulent outflow from the plume mask begins to match the magnitude of the

source (i.e., when the plume is no longer fully contained within the mask). We estimate this stabilization time by visual inspection of the plume masks.

**Acknowledgments**

This work was funded by the NASA Carbon Monitoring System (CMS) and supported by the International Methane Emissions Observatory (IMEO) of the United Nations Environment Programme (UNEP). We thank Antoine Benoit and the Kayrros team for providing their catalog of TROPOMI methane super-emitters.

**References**


1. IPCC, 2021: Climate Change 2021: The Physical Science Basis. Contribution of Working Group I to the Sixth Assessment Report of the Intergovernmental Panel on Climate Change [Masson-Delmotte, V., P. Zhai, A. Pirani, S.L. Connors, C. Péan, S. Berger, N. Caud, Y. Chen, L. Goldfarb, M.I. Gomis, M. Huang, K. Leitzell, E. Lonnoy, J.B.R. Matthews, T.K. Maycock, T. Waterfield, O. Yelekçi, R. Yu, and B. Zhou (eds.)]. Cambridge University Press, Cambridge, United Kingdom and New York, NY, USA, In press, doi:10.1017/9781009157896.
2. Saunois, M., Stavert, A. R., Poulter, B., Bousquet, P., Canadell, J. G., Jackson, R. B., Raymond, P. A., Dlugokencky, E. J., Houweling, S., Patra, P. K., Ciais, P., Arora, V. K., Bastviken, D., Bergamaschi, P., Blake, D. R., Brailsford, G., Bruhwiler, L., Carlson, K. M., Carrol, M., Castaldi, S., Chandra, N., Crevoisier, C., Crill, P. M., Covey, K., Curry, C. L., Etiope, G., Frankenberg, C., Gedney, N., Hegglin, M. I., Höglund-Isaksson, L., Hugelius, G., Ishizawa, M., Ito, A., Janssens-Maenhout, G., Jensen, K. M., Joos, F., Kleinen, T., Krummel, P. B., Langenfelds, R. L., Laruelle, G. G., Liu, L., Machida, T., Maksyutov, S., McDonald, K. C., McNorton, J., Miller, P. A., Melton, J. R., Morino, I., Müller, J., Murguia-Flores, F., Naik, V., Niwa, Y., Noce, S., O'Doherty, S., Parker, R. J., Peng, C., Peng, S., Peters, G. P., Prigent, C., Prinn, R., Ramonet, M., Regnier, P., Riley, W. J., Rosentreter, J. A., Segers, A., Simpson, I. J., Shi, H., Smith, S. J., Steele, L. P., Thornton, B. F., Tian, H., Tohjima, Y., Tubiello, F. N., Tsuruta, A., Viovy, N., Voulgarakis, A., Weber, T. S., van Weele, M., van der Werf, G. R., Weiss, R. F., Worthy, D., Wunch, D., Yin, Y., Yoshida, Y., Zhang, W., Zhang, Z., Zhao, Y., Zheng, B., Zhu, Q., Zhu, Q., and Zhuang, Q.: The Global Methane Budget 2000–2017, Earth Syst. Sci. Data, 12, 1561–1623, https://doi.org/10.5194/essd-12-1561-2020, 2020.
3. Ocko, I. B., Sun, T., Shindell, D., Oppenheimer, M., Hristov, A. N., Pacala, S. W., Mauzerall, D. L., Xu, Y., and Hamburg, S. P.: Acting rapidly to deploy readily available methane mitigation measures by sector can immediately slow global warming, Environ. Res. Lett., 16, 054042, https://doi.org/10.1088/1748-9326/abf9c8, 2021.
4. Jacob, D. J., Turner, A. J., Maasakkers, J. D., Sheng, J., Sun, K., Liu, X., Chance, K., Aben, I., McKeever, J., and Frankenberg, C.: Satellite observations of atmospheric methane and their value for quantifying methane emissions, Atmos. Chem. Phys., 16, 14371–14396, https://doi.org/10.5194/acp-16-14371-2016, 2016.
5. Jacob, D. J., Varon, D. J., Cusworth, D. H., Dennison, P. E., Frankenberg, C., Gautam, R., Guanter, L., Kelley, J., McKeever, J., Ott, L. E., Poulter, B., Qu, Z., Thorpe, A. K., Worden, J. R., and Duren, R. M.: Quantifying methane emissions from the global scale down to point sources using satellite observations of atmospheric methane, Atmos. Chem. Phys., 22, 9617–9646, https://doi.org/10.5194/acp-22-9617-2022, 2022.
6. Vaughn, T. L., Bell, C. S., Pickering, C. K., Schwietzke, S., Heath, G. A., Pétron, G., Zimmerle, D. J., Schnell, R. C., and Nummedal, D.: Temporal variability largely explains top-down/bottom-up difference in methane emission estimates from a natural gas production region, P. Natl. Acad. Sci. USA, 115, 11712–11717, 2018.
7. Cusworth, D. H., Duren, R. M., Thorpe, A. K., Olson-Duvall, W., Heckler, J., Chapman, J. W., Eastwod, M. L., Helmlinger, M. C., Green, R. O., Asner, G. P., Dennison, P. E., and Miller, C. E.: Intermittency of large methane emitters in the Permian Basin, Environ. Sci. Technol. Lett., 8, 567–573, https://doi.org/10.1021/acs.estlett.1c00173, 2021.
8. Lauvaux, T., Giron, C., Mazzolini, M., d'Aspremont, A., Duren, R., Cusworth, D., Shindell, D., and Ciais, P.: Global assessment of oil and gas methane ultra-emitters, Science, 375, 557–561, https://doi.org/10.31223/X5NS54, 2022.
9. Veefkind, J., I. Aben, K. McMullan, H. Förster, J. de Vries, G. Otter, J. Claas, H. J. Eskes, J. F. de Haan, Q. Kleipool, M. van Weele, O. Hasekamp, R. Hoogeveen, J. Landgraf, R. Snel, P. Tol, P. Ingmann, R. Voors, B. Kruizinga, R. Vink, H. Visser, P. F. Levelt, TROPOMI on the ESA Sentinel-5 Precursor: A GMES mission for global observations of the

atmospheric composition for climate, air quality and ozone layer applications. Remote Sens. Environ. 120, 70–83, 2012.
10. Jia, M., Li, F., Zhang, Y., Wu, M., Li, Y., Feng, S., Wang, H., Chen, H., Ju, W., Lin, J., et al.: The Nord Stream pipeline gas leaks released approximately 220,000 tonnes of methane into the atmosphere. Environ. Sci. Ecotechnol., 12, 100210, https://doi.org/10.1016/j.ese.2022.100210, 2022.
11. U. S. Energy Information Administration (EIA): U.S. natural gas exports to Mexico set to rise with completion of the Wahalajara system, https://www.eia.gov/todayinenergy/detail.php?id=44278 (last access: 4 June 2023), 2020.
12. Farzaneh-Gord, M., Mohammad Sadegh Pahlevan-Zadeh, Amir Ebrahimi-Moghadam, Saied Rastgar, Measurement of methane emission into environment during natural gas purging process, Environmental Pollution, Volume 242, Part B, Pages 2014-2026, ISSN 0269-7491, 2018.
13. Alvarez, R. A., Zavala-Araiza, D., Lyon, D. R., Allen, D. T., Barkley, Z. R., Brandt, A. R., Davis, K. J., Herndon, S. C., Jacob, D. J., Karion, A., Kort, E. A., Lamb, B. K., Lauvaux, T., Maasakkers, J. D., Marchese, A. J., Omara, M., Pacala, S. W., Peischl, J., Robinson, A. L., Shepson, P. B., Sweeney, C., Townsend-Small, A., Wofsy, S. C., and Hamburg, S. P.: Assessment of methane emissions from the U.S. oil and gas supply chain, Science, 361, 186–188, https://doi.org/10.1126/science.aar7204, 2018.
14. Molar-Cruz, A., S.A. Huezo Rodríguez, T. Hamacher: Characterizing the energy burden of urban households in Mexico: The impact of socioeconomic and temperature conditions across Metropolitan Areas, Frontiers in Sustainable Cities, p. 3, https://www.frontiersin.org/article/10.3389/frsc.2021.662968, 2022.
15. Bessho, K., Date, K., Hayashi, M., Ikeda, A., Imai, T., Inoue, H., Kumagai, Y., Miyakawa, T., Murata, H., Ohno, T., Okuyama, A., Oyama, R., Sasaki, Y., Shimazu, Y., Shimoji, K., Sumida, Y., Suzuki, M., Taniguchi, H., Tsuchiyama, H., Uesawa, D., Yokota, H., & Yoshida, R.: An introduction to Himawari-8/9—Japan's new-generation geostationary meteorological satellites. Journal of the Meteorological Society of Japan, 94, 151– 183. https://doi.org/10.2151/jmsj.2016-009, 2016.
16. Holmlund, K., and Coauthors: Meteosat Third Generation (MTG): Continuation and Innovation of Observations from Geostationary Orbit. Bull. Amer. Meteor. Soc., 102, E990–E1015, https://doi.org/10.1175/BAMS-D-19-0304.1, 2021.
17. Moore B III, Crowell SMR, Rayner PJ, Kumer J, O'Dell CW, O'Brien D, Utembe S, Polonsky I, Schimel D and Lemen J: The Potential of the Geostationary Carbon Cycle Observatory (GeoCarb) to Provide Multi-scale Constraints on the Carbon Cycle in the Americas. Front. Environ. Sci. 6:109. doi: 10.3389/fenvs.2018.00109, 2018.
18. Schmit, T. J., P. Griffith, M. M. Gunshor, J. M. Daniels, S. J. Goodman, and W. J. Lebair, 2017: A Closer Look at the ABI on the GOES-R Series. Bull. Amer. Meteor. Soc., 98, 681–698, https://doi.org/10.1175/BAMS-D-15-00230.1, 2017.
19. Gordon, I. E., Rothman, L. S., Hill, C., Kochanov, R. V., Tan, Y., Bernath, P. F., Birk, M., Boudon, V., Campargue, A., Chance, K. V., Drouin, B. J., Flaud, J.-M., Gamache, R. R., Hodges, J. T., Jacquemart, D., Perevalov, V. I., Perrin, A., Shine, K. P., Smith, M.-A. H., Tennyson, J., Toon, G. C., Tran, H., Tyuterev, V. G., Barbe, A., Császár, A. G., Devi, V. M., Furtenbacher, T., Har- rison, J. J., Hartmann, J.-M., Jolly, A., Johnson, T. J., Karman, T., Kleiner, I., Kyuberis, A. A., Loos, J., Lyulin, O. M., Massie, S. T., Mikhailenko, S. N., Moazzen-Ahmadi, N., Müller, H. S. P., Naumenko, O. V., Nikitin, A. V., Polyansky, O. L., Rey, M., Rotger, M., Sharpe, S. W., Sung, K., Starikova, E., Tashkun, S. A., Auwera, J. V., Wagner, G., Wilzewski, J., Wcisło, P., Yu, S., and Zak, E. J.: The HITRAN2016 Molecular

Spectro- scopic Database, J. Quant. Spectrosc. Radiat. Transf., 203, 3–69, https://doi.org/10.1016/j.jqsrt.2017.06.038, 2017.
20. Kochanov, R. V., Gordon, I. E., Rothman, L. S., Wcisło, P., Hill, C., and Wilzewski, J. S.: HITRAN Application Programming Interface (HAPI): A comprehensive approach to working with spectroscopic data, J. Quant. Spectrosc. Radiat. Transf., 177, 15–30, 2016.
21. Varon, D. J., D. Jervis, J. McKeever, I. Spence, D. Gains, and D. J. Jacob. High-frequency monitoring of anomalous methane point sources with multispectral sentinel-2 satellite observations. Atmospheric Measurement Techniques, 14(4):2771–2785, 2021.
22. Irakulis-Loitxate, I., Guanter, L., Maasakkers, J. D., Zavala-Araiza, D., and Aben, I.: Satellites detect abatable super-emissions in one of the world's largest methane hotspot regions, Environ. Sci. Technol. 56, 4, 2143–2152, https://doi.org/10.1021/acs.est.1c04873, 2022.
23. Pandey, S., Nistelrooij, M.V., Maasakkers, J.D., Sutar, P., Houweling, S., Varon, D.J., Tol, P.J., Gains, D., Worden, J.R., & Aben, I.: Daily detection and quantification of methane leaks using Sentinel-3: a tiered satellite observation approach with Sentinel-2 and Sentinel-5p, 2022.
24. Anderson, G., Clough, S., Kneizys, F., Chetwynd, J., and Shettle, E.: AFGL atmospheric constituent profiles (0–120 km), Tech. Rep. AFGL-TR-86-0110, Air Force Geophys. Lab., Hanscom Air Force Base, Bedford, Mass., USA, 1986.
25. Wang, Z., A. C. Bovik, H. R. Sheikh and E. P. Simoncelli, "Image quality assessment: from error visibility to structural similarity," in IEEE Transactions on Image Processing, vol. 13, no. 4, pp. 600-612, April 2004, doi: 10.1109/TIP.2003.819861, 2004.
26. Groshenry, A., Clement Giron, Thomas Lauvaux, Alexandre d'Aspremont, and Thibaud Ehret. Detecting methane plumes using Prisma: Deep learning model and data augmentation, 2022.
27. Frankenberg, C., Thorpe, A. K., Thompson, D. R., Hulley, G., Kort, E. A., Vance, N., Borchardt, J., Krings, T., Gerilowski, K., Sweeney, C., Conley, S., Bue, B. D., Aubrey, A. D., Hook, S., and Green, R. O.: Airborne methane remote measurements reveal heavy-tail flux distribution in Four Corners region, P. Natl. Acad. Sci. USA, 113, 9734–9739, https://doi.org/10.1073/pnas.1605617113, 2016.
28. Varon, D. J., Jacob, D. J., McKeever, J., Jervis, D., Durak, B. O. A., Xia, Y., and Huang, Y.: Quantifying methane point sources from fine-scale satellite observations of atmospheric methane plumes, Atmos. Meas. Tech., 11, 5673– 5686, https://doi.org/10.5194/amt-11-5673-2018 , 2018.
29. Gorroño, J., Varon, D. J., Irakulis-Loitxate, I., and Guanter, L.: Understanding the potential of Sentinel-2 for monitoring methane point emissions, Atmos. Meas. Tech., 16, 89–107, https://doi.org/10.5194/amt-16-89-2023, 2023.
30. Molod, A.; Takacs, L.; Suarez, M.; Bacmeister, J.; Song, I.-S.; Eichmann, A. The GEOS-5 Atmospheric General Circulation Model: Mean Climate and Development from MERRA to Fortuna; NASA TM-2012-104606; NASA, 2012.

**Figures and Tables**

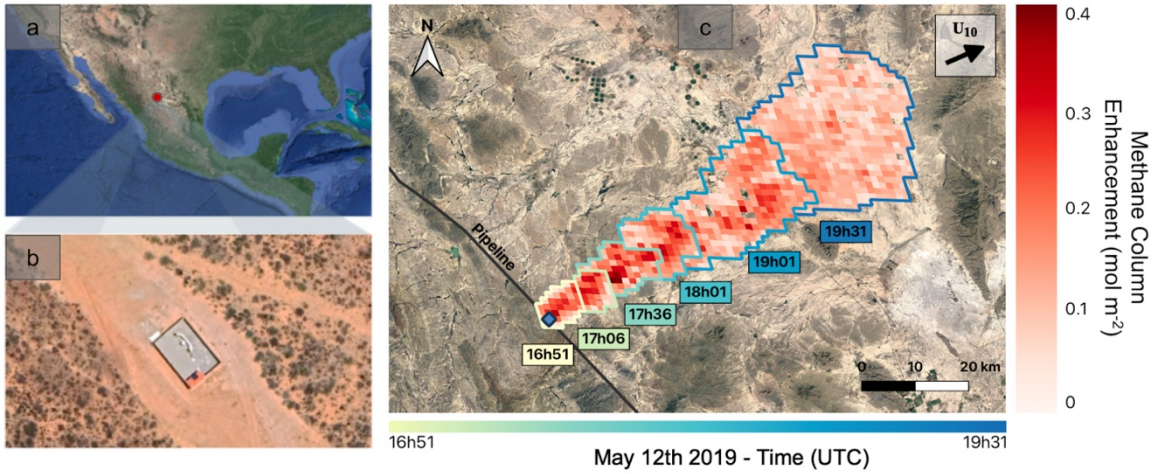


**Figure 1.** Surface imagery for the scene of interest near the El Encino – La Laguna (EELL) natural gas pipeline in northern Mexico, and temporal evolution of the methane plume observed by GOES on 12 May 2019. (a) Location of the source in Durango, Mexico. (b) The pipeline block valve station that produced the emission (26.08580°N, 104.31682°W). (c) Temporal progression of the methane plume illustrated by 5 selected snapshots from 16:51 to 19:31 UTC on 12 May 2019. The snapshots are overlaid in reverse chronological order (earliest on top) and outlined according to acquisition time. The wind vector is for the 10-m wind from the GEOS-FP meteorological reanalysis product at 0.25° × 0.3125° resolution (Molod et al., 2012). The pipeline path (black line) is from the Global Energy Monitor Wiki (May 2023), and background imagery is from © (2023) Google Earth.

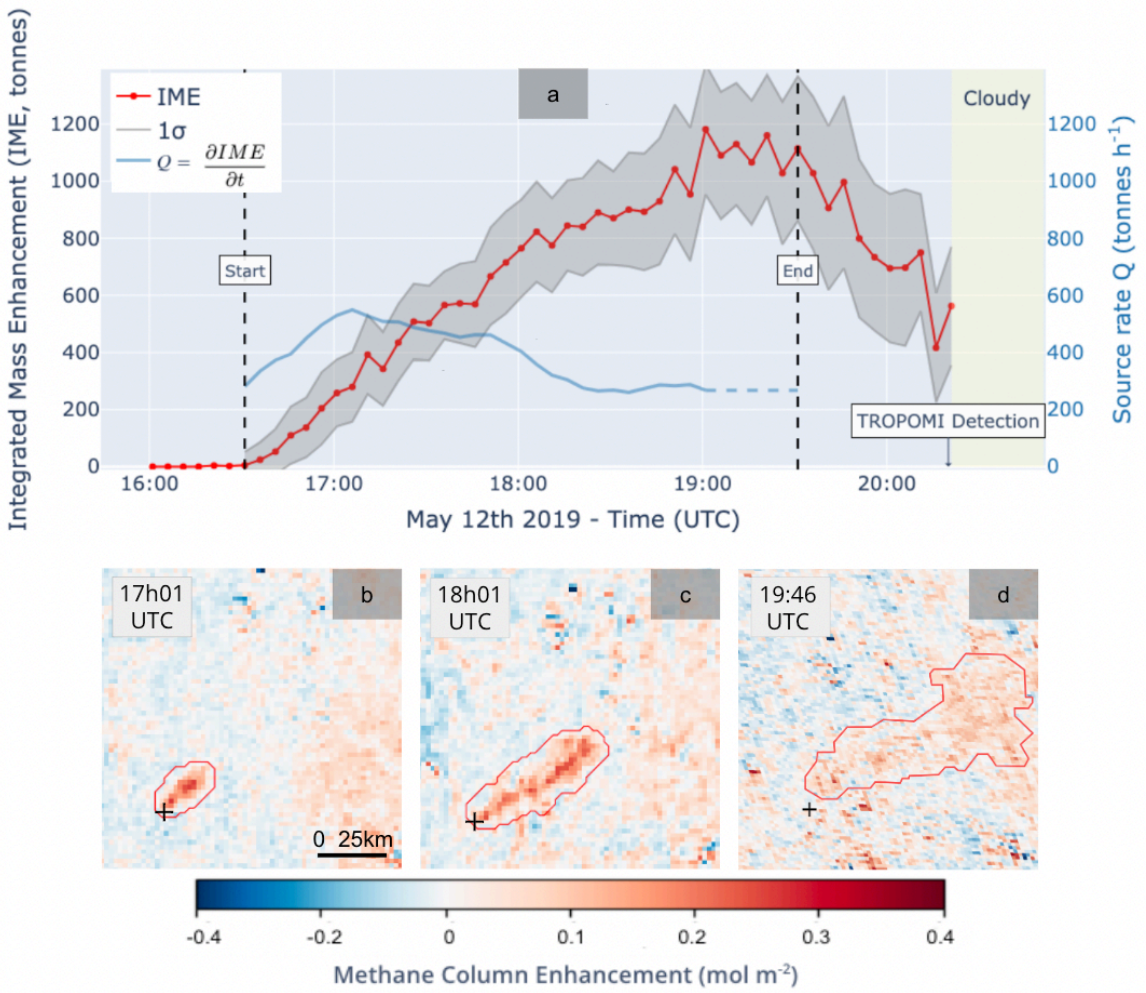


**Figure 2.** GOES source rate quantification and methane plume retrievals for the Durango EELL pipeline source of Figure 2 on 12 May 2019. (a) 5-minute evolution of the integrated methane enhancement (IME) from which the source rate is inferred. The red line shows the evolution of the IME from the sequence of plume images and the gray envelope gives the associated 1-sigma uncertainty. The blue line estimates the time-dependent source rate Q (right axis) as the trend of a 5-point moving average of the IME from 16:30 to 19:00 UTC, with the dashed segment indicating extrapolation. The dashed vertical lines mark the start and end of the release. (b–d) Sample methane retrieval fields and plume masks (red contour lines) showing the temporal evolution of the imaged plume from 17:01 to 19:01 UTC.

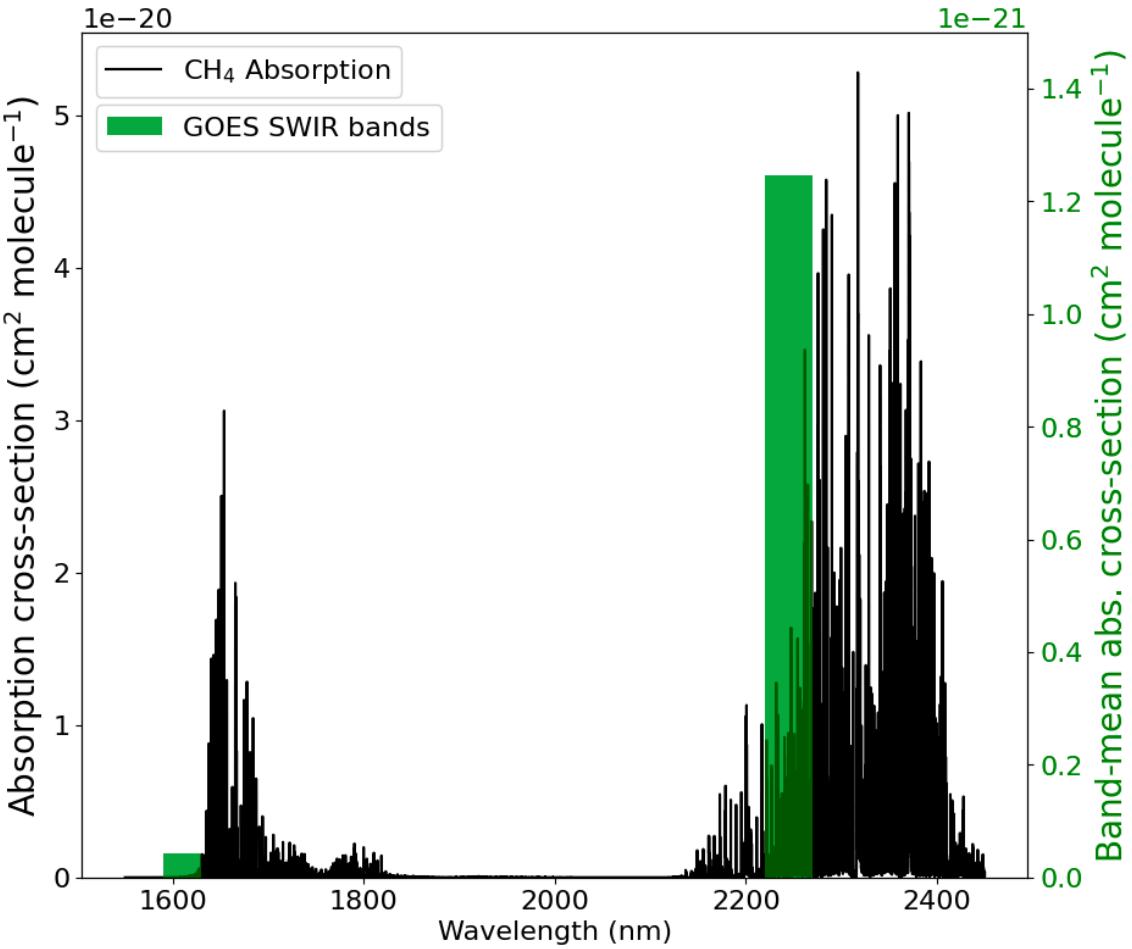


**Figure 3.** Methane absorption cross-sections and GOES bands (5 and 6) in the SWIR spectral range. The absorption cross-sections (left axis) are from HITRAN2016 line spectra convolved with a Voigt profile. The mean absorption cross-section in each GOES band is plotted on the right axis.

**Supporting information**

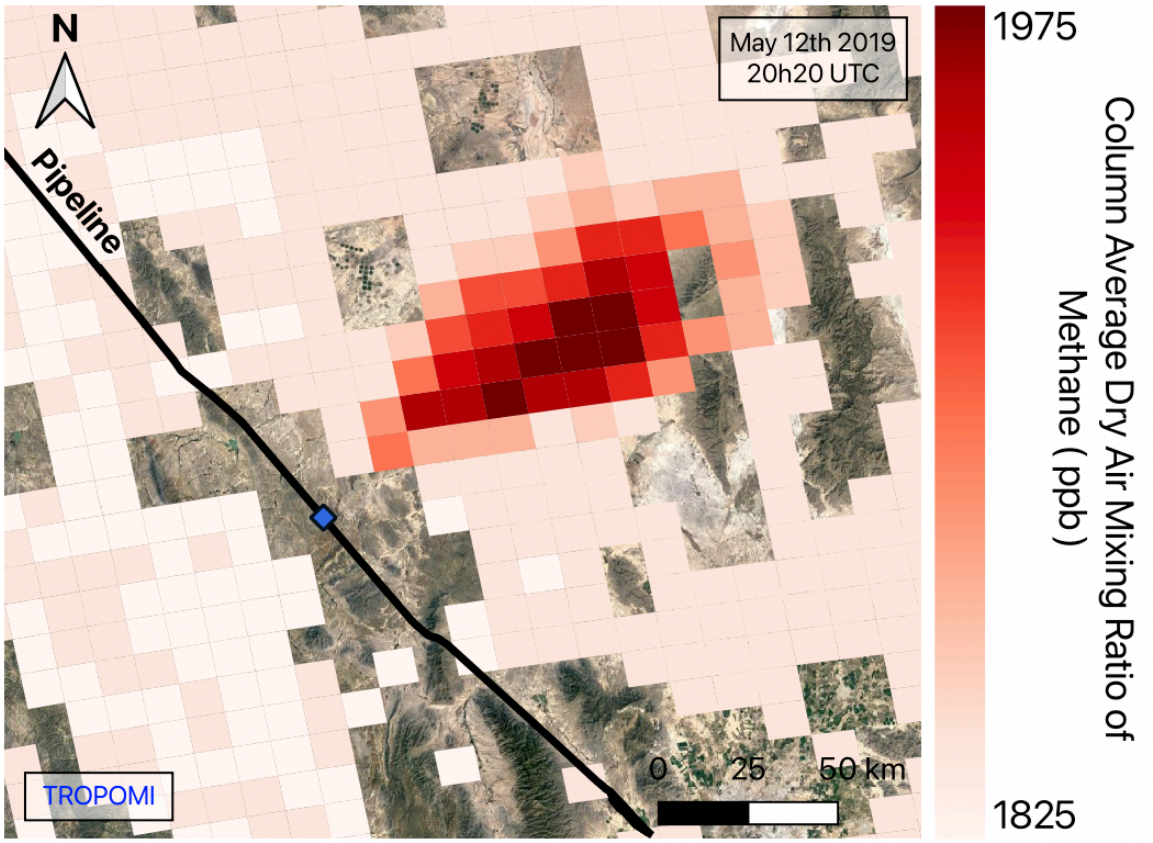


**Figure S1.** Methane plume from the EELL pipeline observed by TROPOMI (v02.04.00 operational data product) on 12 May 2019 at 20:20 UTC (15:20 local time), overlaid on surface imagery from © (2023) Google Earth.

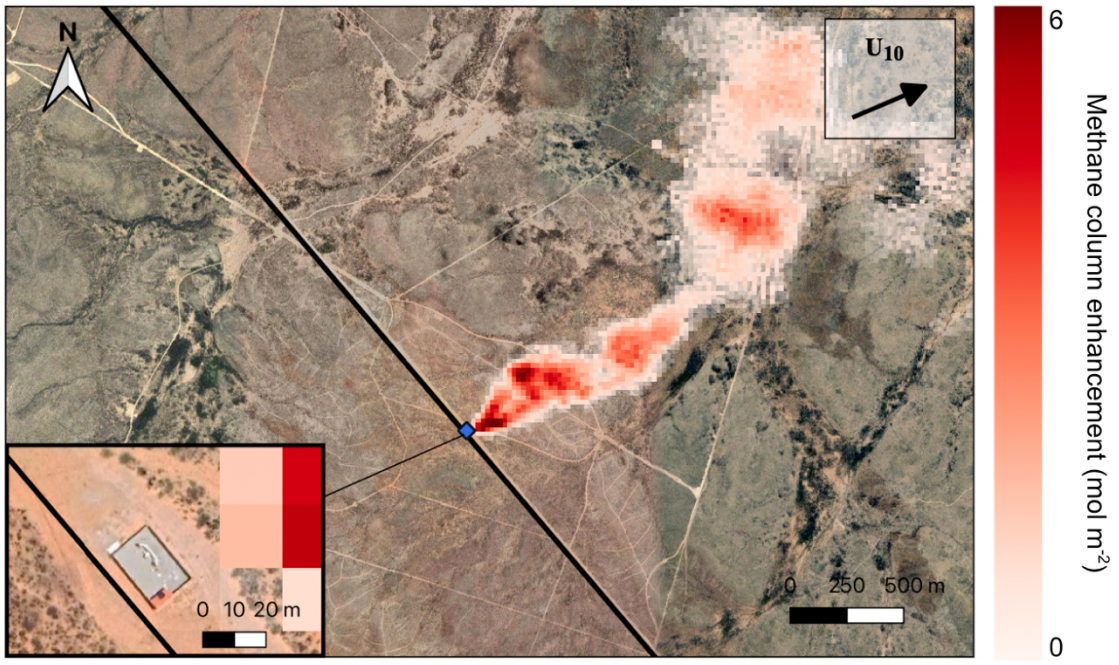


**Figure S2.** Sentinel-2 detection of large methane emissions from the EELL block valve station at (26.08580°N, 104.31682°W) on 11 May 2019 (12:46 local time). The methane retrieval was performed using the multi-band–multi-pass (MBMP) method (Varon et al., 2021; Irakulis-Loitxate et al., 2022). The emission was quantified at 551 ± 229 t $h^{-1}$ by the IME method (Varon et al., 2018). Background image is from © (2023) Google Earth.

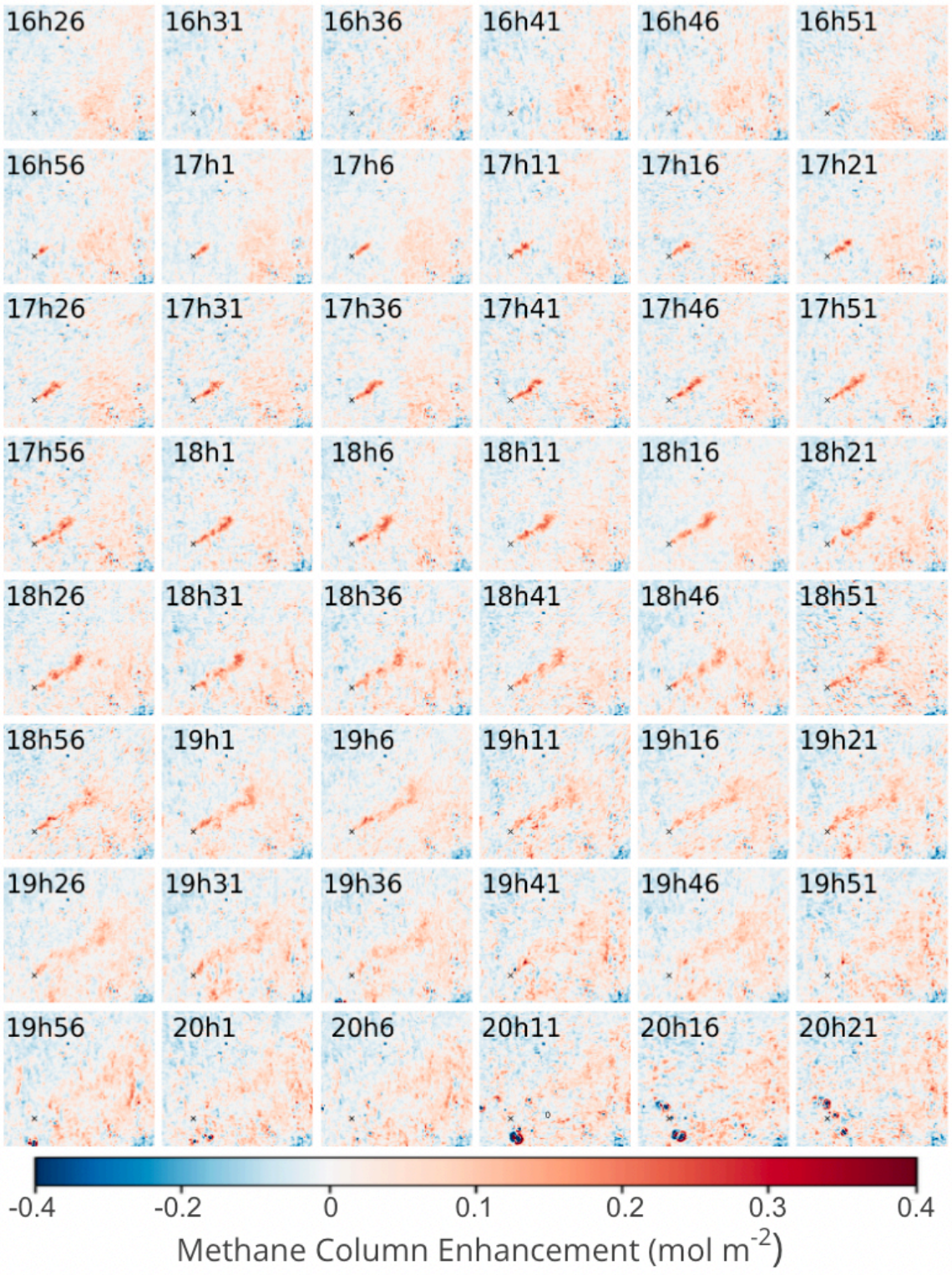


**Figure S3.** 48 snapshots of the EELL methane plume over the course of the 12 May 2019 release, from 16:26 to 20h21 UTC. The black x marks the source location. We estimate the release began at 16:30 UTC and ended at 19:30 UTC, after which point the plume detaches from the source.

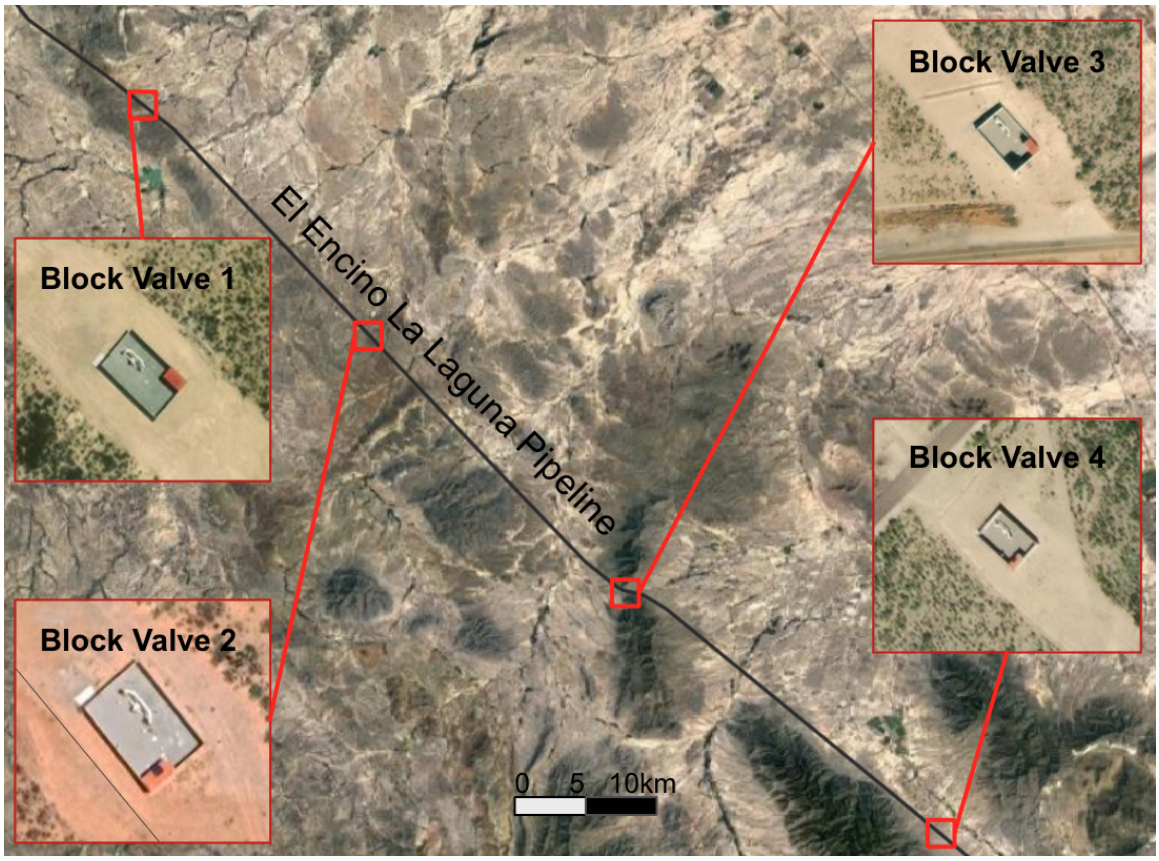


**Figure S4.** Four block valve stations analyzed with GOES on dates with TROPOMI or Sentinel-2 detections. They are spaced by roughly 30 km and located, from North to South, at (26.297686°N, -104.530079°W), (26.085840°N, -104.316830°W), (25.873025°N, -104.105993°W) and (25.681875°N, -103.855128°W). Block valve station 2 was the source of the large release detected by GOES on 12 May 2019. Background imagery is from © (2023) Google Earth.

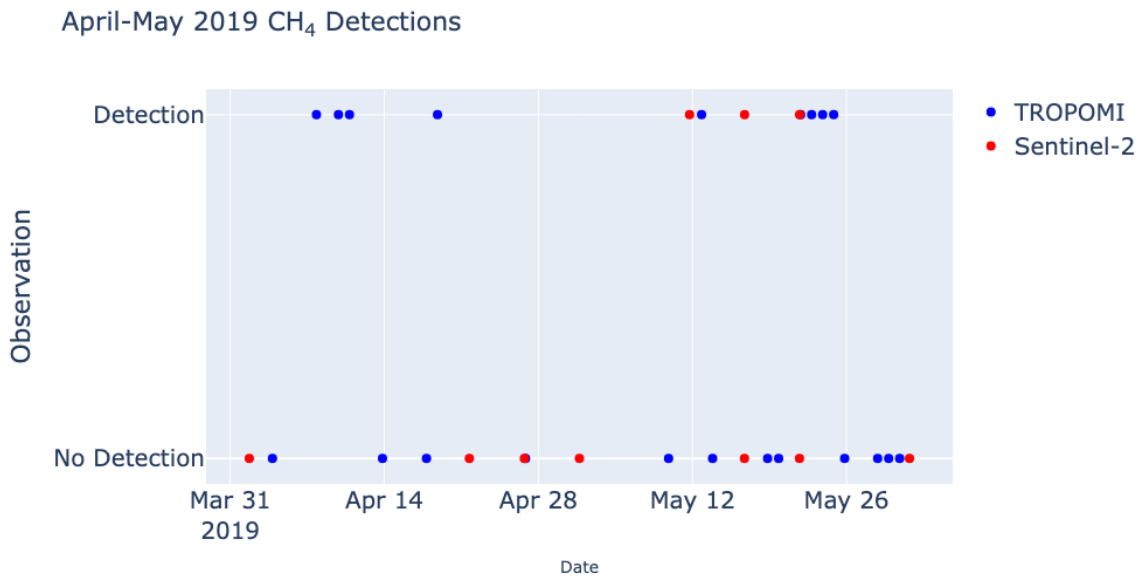


**Figure S5.** Temporal analysis of TROPOMI and Sentinel-2 detections/non-detections of EELL pipeline sources on cloud-free passes during April-May 2019. TROPOMI and Sentinel-2 detected large methane plumes on a combined 12 of 31 cloud-free passes. TROPOMI detections are based on the v02.04.00 operational data product. Sentinel-2 detections are based on the multi-band–multi-pass (MBMP) retrieval method (Varon et al., 2021; Irakulis-Loitxate et al., 2022).

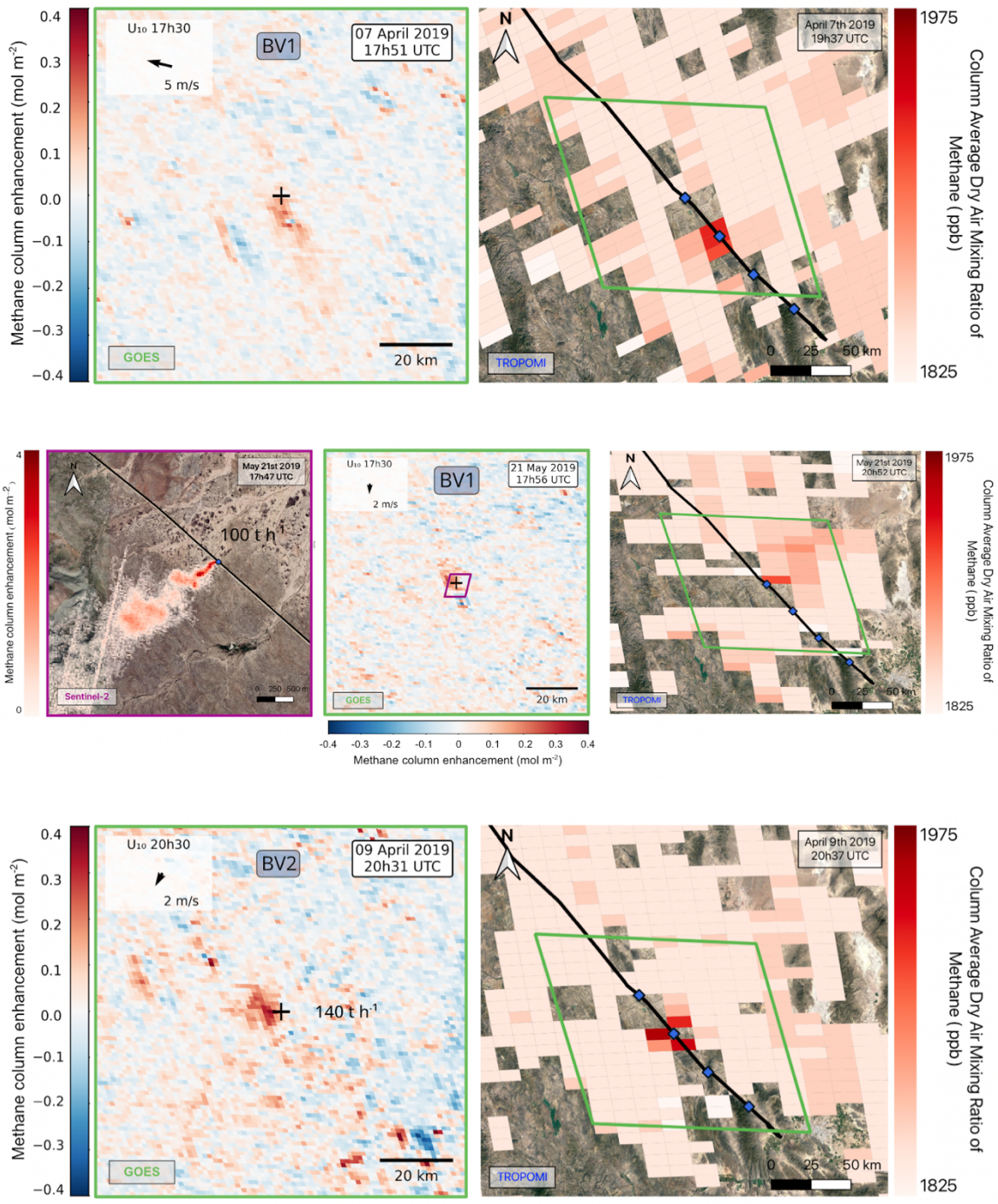
U10 17h30
5 m/s
BV1
07 April 2019
17h51 UTC
GOES
20 km
Methane column enhancement (mol m-2)
0.4
0.3
0.2
0.1
0.0
−0.1
−0.2
−0.3
−0.4
N
April 7th 2019
19h37 UTC
TROPOMI
0 25 50 km
1975
1825
Column Average Dry Air Mixing Ratio of Methane (ppb)
May 21st 2019
17h47 UTC
100 t h-1
Sentinel-2
U10 17h30
2 m/s
BV1
21 May 2019
17h56 UTC
GOES
20 km
May 21st 2019
20h52 UTC
TROPOMI
-0.4 -0.3 -0.2 -0.1 0 0.1 0.2 0.3 0.4
Methane column enhancement (mol m-2)
U10 20h30
2 m/s
BV2
09 April 2019
20h31 UTC
140 t h-1
GOES
20 km
April 9th 2019
20h37 UTC
TROPOMI

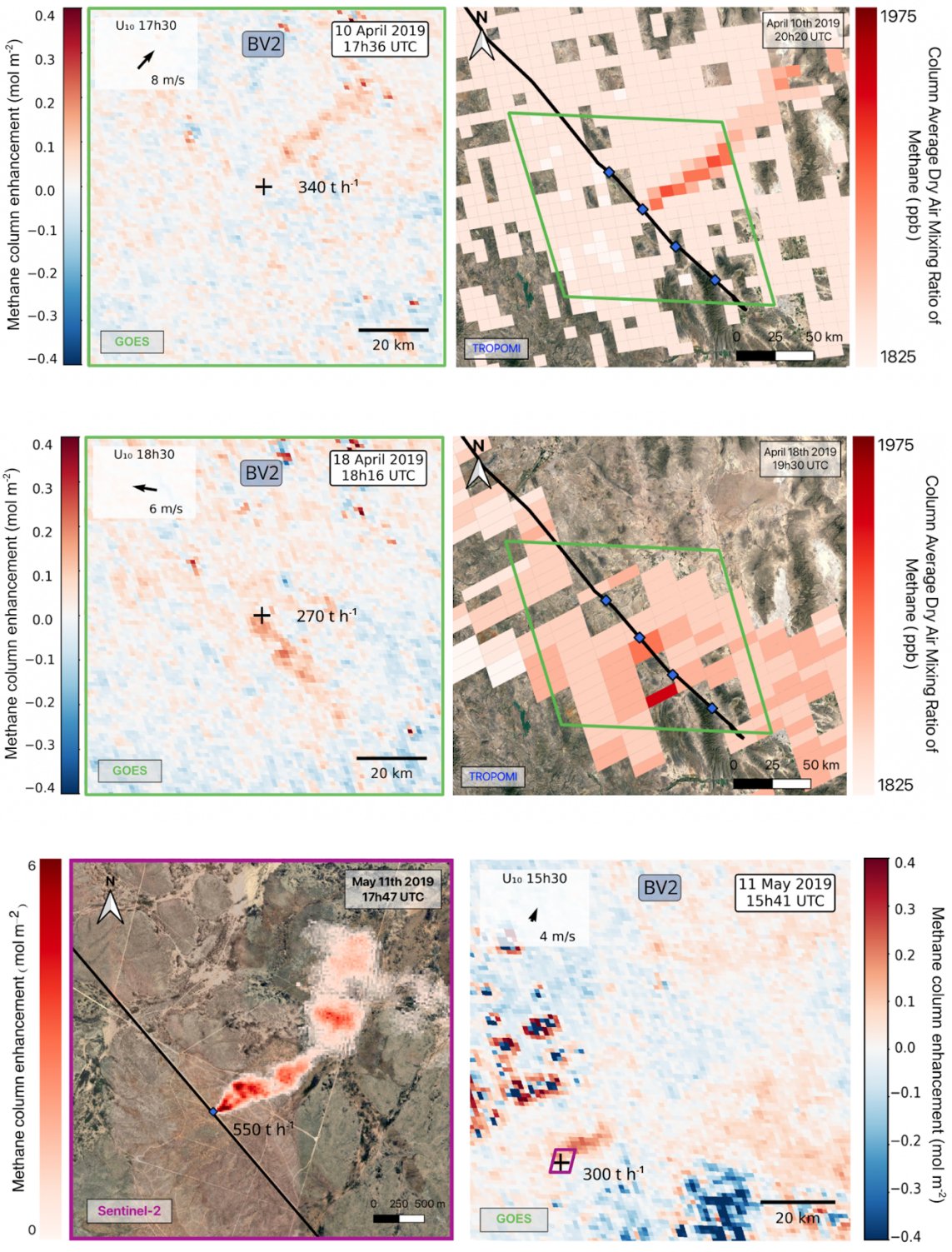
Methane column enhancement (mol m-2)
0.4
0.3
0.2
0.1
0.0
−0.1
−0.2
−0.3
−0.4
U10 17h30
8 m/s
BV2
10 April 2019
17h36 UTC
340 t h-1
GOES
20 km
N
April 10th 2019
20h20 UTC
TROPOMI
0 25 50 km
1975
1825
Column Average Dry Air Mixing Ratio of Methane (ppb)
U10 18h30
6 m/s
BV2
18 April 2019
18h16 UTC
270 t h-1
GOES
20 km
N
April 18th 2019
19h30 UTC
TROPOMI
0 25 50 km
1975
1825
Column Average Dry Air Mixing Ratio of Methane (ppb)
Methane column enhancement (mol m-2)
6
0
N
May 11th 2019
17h47 UTC
550 t h-1
Sentinel-2
0 250 500 m
U10 15h30
4 m/s
BV2
11 May 2019
15h41 UTC
300 t h-1
GOES
20 km
0.4
0.3
0.2
0.1
0.0
−0.1
−0.2
−0.3
−0.4
Methane column enhancement (mol m-2)

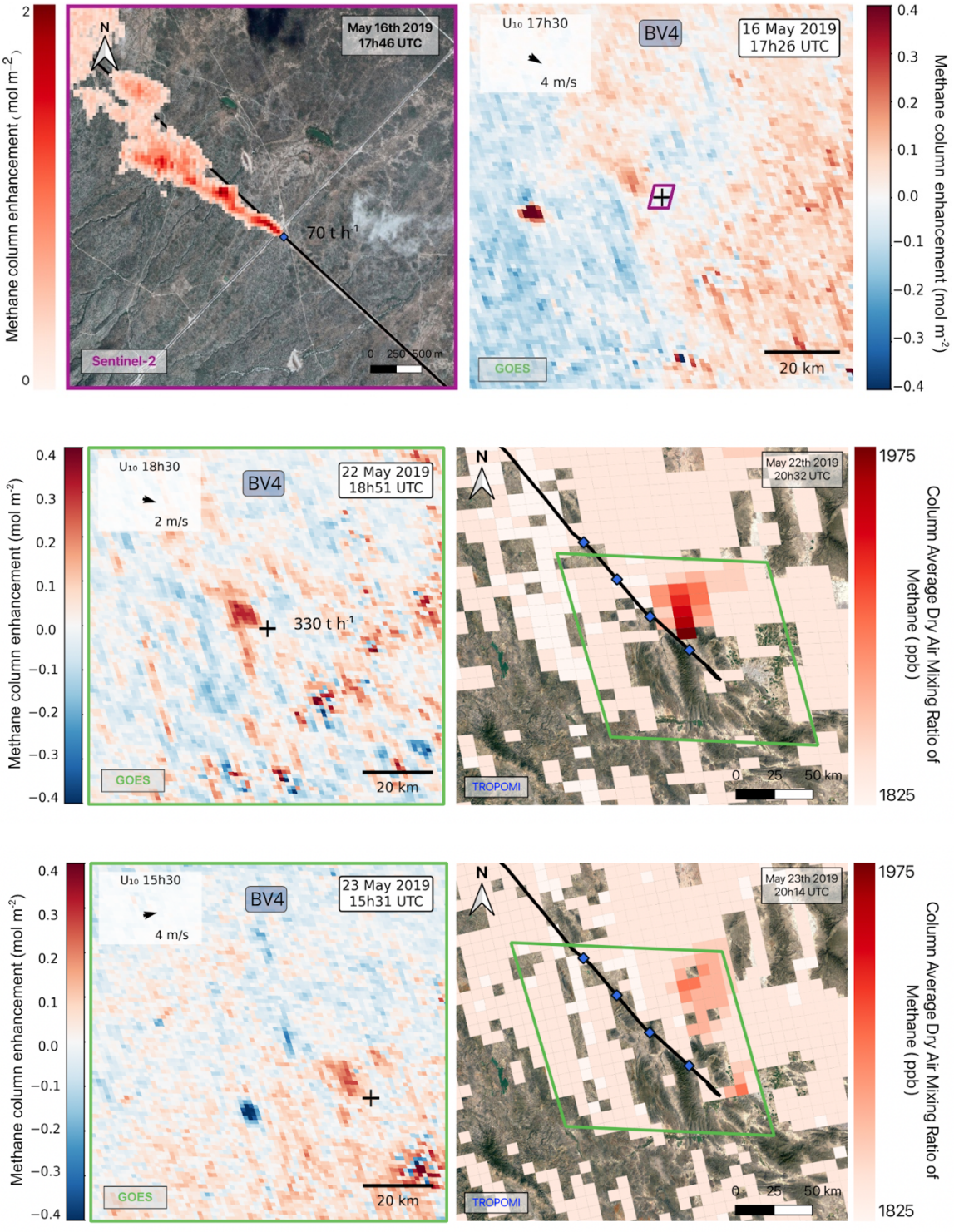
Methane column enhancement (mol m-2)
2
0
N
May 16th 2019
17h46 UTC
70 t h-1
Sentinel-2
0 250 500 m
U10 17h30
4 m/s
BV4
16 May 2019
17h26 UTC
GOES
20 km
0.4
0.3
0.2
0.1
0.0
−0.1
−0.2
−0.3
−0.4
Methane column enhancement (mol m-2)
U10 18h30
2 m/s
BV4
22 May 2019
18h51 UTC
330 t h-1
GOES
20 km
N
May 22th 2019
20h32 UTC
TROPOMI
0 25 50 km
1975
1825
Column Average Dry Air Mixing Ratio of Methane (ppb)
U10 15h30
4 m/s
BV4
23 May 2019
15h31 UTC
GOES
20 km
N
May 23th 2019
20h14 UTC
TROPOMI
0 25 50 km

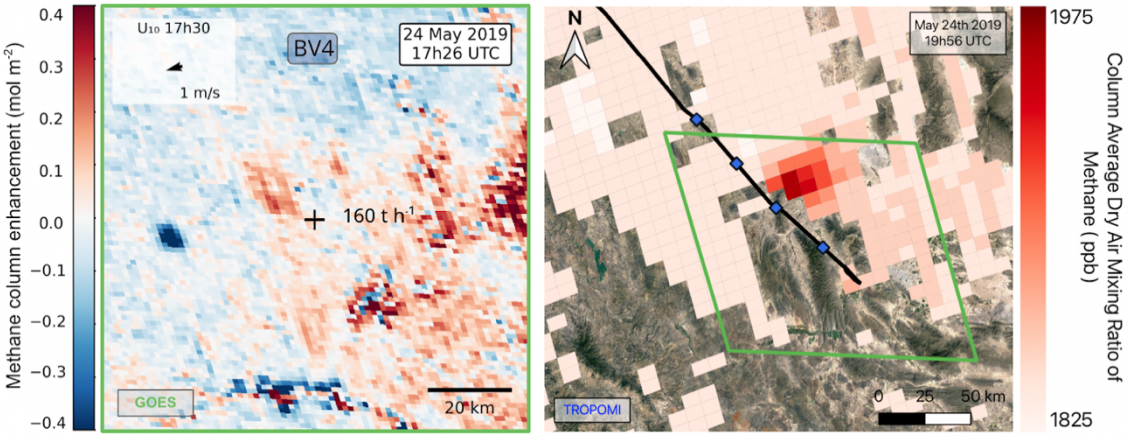


**Figure S6.** GOES, Sentinel-2, and TROPOMI methane plume detections from block valve stations 1 (BV1), 2 (BV2) and 4 (BV4) in April and May 2019 (see Fig. S4, S5), in addition to the 12 May 2019 detection discussed in the main text. No plumes were observed from block valve station 3 (Fig. S4). TROPOMI data are from the v02.04.00 operational data product. Sentinel-2 detections are based on the multi-band–multi-pass (MBMP) retrieval method (Varon et al., 2021; Irakulis-Loitxate et al., 2022). Source rates (inset) are reported from IME linear regressions during cloud-free periods where possible for GOES retrievals, and using the wind-based IME method (Varon et al., 2018) for Sentinel-2 retrievals. GOES imaging domains are shown as green inset boxes in TROPOMI scenes; Sentinel-2 imaging domains are shown as pink inset boxes in GOES domains. Wind insets show the 10-m wind from GEOS-FP.